Interaction of ICRF Fields with the Plasma Boundary in AUG and JET and Guidelines for Antenna Optimization

V. Bobkov, R. Bilato, F. Braun, L. Colas, R. Dux et al.

Citation: AIP Conf. Proc. **1187**, 125 (2009); doi: 10.1063/1.3273710
View online: http://dx.doi.org/10.1063/1.3273710
View Table of Contents: http://proceedings.aip.org/dbt/dbt.jsp?KEY=APCPCS&Volume=1187&Issue=1
Published by the American Institute of Physics.

Interaction of ICRF Fields with the Plasma Boundary in AUG and JET and Guidelines for Antenna Optimization

V. Bobkov[a], R. Bilato[a], F. Braun[a], L. Colas[b], R. Dux[a], D. Van Eester[c], L. Giannone[a], M. Goniche[b], A. Herrmann[a], P. Jacquet[d], A. Kallenbach[a], A.Krivska[e,f], E. Lerche[c], M.-L. Mayoral[d], D. Milanesio[g], I. Monakhov[d], H.W. Müller[a], R. Neu[a], J.-M. Noterdaeme[a,h], Th. Pütterich[a], V. Rohde[a], ASDEX Upgrade Team and JET-EFDA Contributors*

[a]*Max-Planck-Institut für Plasmaphysik, EURATOM Association, Garching, Germany*
[b]*CEA, IRFM, F-13108 Saint-Paul-lez-Durance, France;*
[c]*ERM-KSN EURATOM Association–Belgian State, Brussels, Belgium;*
[d]*EURATOM/UKAEA, Culham Science Centre, OX14 3DB, Abingdon, UK ;*
[e]*Institute of Plasma Physics ASCR, Euratom Association, Za Slovankou 3, Prague, Czech Republic;*
[f]*Czech Technical University, Telecommunication Engineering Department, Prague, Czech Republic;*
[g]*Department of Electronics, Politecnico di Torino, Torino, Italy*
[h]*Gent University, EESA Department, Gent, Belgium*

Abstract. *W* sputtering during ICRF on ASDEX Upgrade (AUG) and temperature rise on JET A2 antenna septa are considered in connection with plasma conditions at the antenna plasma facing components and $E_{||}$ near-fields. Large antenna-plasma clearance, high gas puff and low light impurity content are favorable to reduce *W* sputtering in AUG. The spatial distribution of spectroscopically measured effective *W* sputtering yields clearly points to the existence of strong $E_{||}$ fields at the antenna box ("feeder fields") which dominate over the fields in front of the antenna straps. The picture of $E_{||}$ fields, obtained by HFSS code, corroborates the dominant role of $E_{||}$ at the antenna box on the formation of sheath-driving RF voltages for AUG. Large antenna-plasma clearance and low gas puff are favorable to reduce septum temperature of JET A2 antennas. Assuming a linear relation between the septum temperature and the sheath driving RF voltage calculated by HFSS, the changes of the temperature with dipole phasing ($00\pi\pi$, $0\pi\pi0$ or $0\pi0\pi$) are well described by the related changes of the RF voltages. Similarly to the AUG antenna, the strongest $E_{||}$ are found at the limiters of the JET A2 antenna for all used dipole phasings and at the septum for the phasings different from $0\pi0\pi$.
A simple general rule can be used to minimize $E_{||}$ at the antenna: image currents can be allowed only at the surfaces which do not intersect magnetic field lines at large angles of incidence. Possible antenna modifications generally rely either on a reduction of the image currents, on their short-circuiting by introducing additional conducting surfaces or on imposing the $E_{||}$=0 boundary condition. On the example of AUG antenna, possible options to minimize the sheath driving voltages are presented.

Keywords: ASDEX-Upgrade, JET, ICRF, High-Z Material, Hot spots, Impurity Sources
PACS: 52.50.G, 52.40.F, 52.40.H

During the use of Ion Cyclotron Range of Frequencies (ICRF) systems in magnetic fusion devices, interaction between RF fields and the plasma facing components (PFCs) can lead to operational issues. Since the installation of *W*-coated limiters in ASDEX Upgrade (AUG) [1], *W* release during ICRF operation has made ICRF operation in high performance discharges difficult. On JET, noticeable temperature rises on

CP1187, *Radio Frequency Power in Plasmas*
edited by V. Bobkov and J.-M. Noterdaeme

the A2 antennas septa [2] were observed using infra-red imaging. These increases, although less problematic with the present septa material (CFC), are a concern for future operation with septa made of beryllium. The effects can be attributed to existence of strong near-antenna $E_{||}$-fields and related sheath effects. To reduce the effects for the next generation of ICRF antennas, the most important plasma parameters and origins of $E_{||}$-fields need to be better identified. We describe empirical dependencies of ICRF-related W sputtering in AUG (summarizing [2,3]) and PFC heat deposition in JET on plasma parameters, identify the most probable sources of $E_{||}$-fields, and describe possible steps to reduce these fields.

EMPIRICAL DEPENDENCIES ON PLASMA PARAMETERS

In AUG, data from spectroscopically measured W sputtering yield Y_W at plasma facing components shows that W is predominantly sputtered by light impurities and not by deuterons [5]. The same applies during ICRF operation. Figure 1 demonstrates the effect of impurity content on the voltage dependence of Y_W for the concentrations spectroscopically measured in a discharge before the boronizations (*gray*, pure W limiters - boron cleaned from surfaces) and in a discharge long after boronizations (*black*, pure W limiters - boron layers eroded [6]). Solid lines correspond to the minimal possible charge state while the dashed lines to the maximum possible charge states obtainable during ELMs. With and without ICRF, a major part of W source is sputtered during ELMs [5]. Average values of Y_W, measured at the limiter of active antenna for both discharges and shown as horizontal lines in Fig. 1, suggest a significant reduction of the ICRF-related W sputtering after the reduction of light impurity content. Measured Y_W values suggest rectified potentials in the range 30-50 V which are in line with the indicative measurements of floating potential in the range V_{fl}=30-100 V on the field lines connected to another 0.5 MW powered antenna.

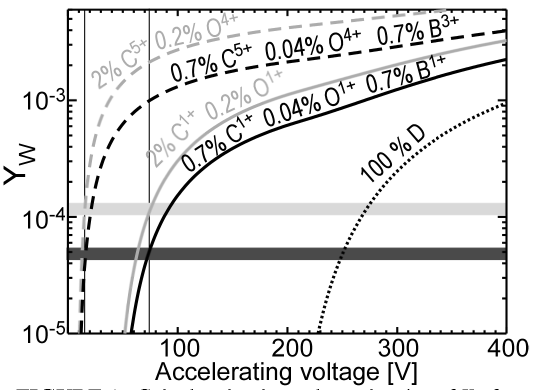

FIGURE 1. Calculated voltage dependencies of Y_W for light impurity content for #23057 (*gray*) and for #23517 (*black*). Horizontal lines show Y_W measured at limiter of an antenna with P_{ICRF}=0.5 MW for these two discharges.

Increasing the plasma-antenna clearance is an effective method to reduce the ICRF-related W influx Γ_W and the sputtering yield Y_W at antenna limiters (the most important W source [5]) in AUG as well as to reduce the ICRF-related temperature rise on the A2 antenna septum in JET [7]. However, the ICRF-related impurity problem described by a change of impurity concentration in the plasma can not be considered on the same terms as the problem of increased power flux due to ICRF. This is demonstrated in Fig. 2 where the AUG time traces of Y_W at the antenna limiter, W concentration C_W at the plasma edge and product of primary flux Γ_D at the antenna limiter and strap voltage V_{RF} are shown during an additional deuterium gas puff. On one hand, a significant

reduction of Y_W and C_W is observed. On the other hand, the increased $\Gamma_D \cdot V_{RF}$ product speaks for higher heat loads at the antenna PFCs. JET data in [7] shows the correlation between $\Gamma_D \cdot V_{RF}$ and A2 antenna septum temperature. Although V_{RF} is not a perfect representative of rectified voltage on the field lines hitting the antenna PFCs, this means that the conditions required to reduce the impurity problem are not necessarily those required to reduce the heat flux problem, although both problems originate to a large extent from $E_{||}$-fields. For example, in contrast to the heat flux, W release depends strongly on the light impurity concentrations and charge states (Fig. 2) which are decreased by the gas puff. Unless a self-amplifying interaction between the plasma and $E_{||}$-fields takes place due to additional gas puff, the latter can be considered as a tool to reduce the impurity problem and improve ICRF coupling at the same time. This happens however at the expense of increased heat flux to antenna PFCs.

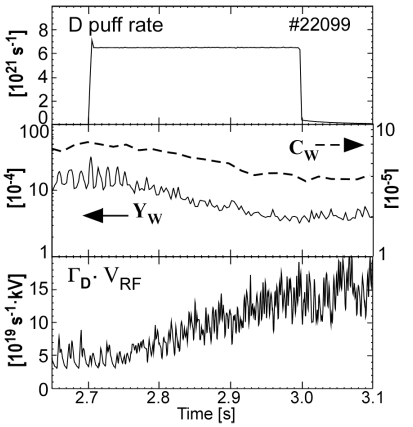

FIGURE 2. Effect of additional D puff in AUG, as a demonstration of de-coupling between impurity and heat flux problems.

ORIGINS OF PARALLEL RF ELECTRIC FIELDS $E_{||}$

As has been described in [8,9], for an antenna geometry which protrudes towards a plasma in the radial direction, the near-antenna $E_{||}$-fields are formed not only by the contributions coming directly from straps of the antenna and their RF magnetic flux, but also by the so-called "feeder" (or "box") fields, which are located on the structures surrounding antenna straps. These two types of fields have different origins and require different approaches for minimization.

ASDEX Upgrade two-strap antenna

In AUG experiments, screening of strap $E_{||}$-contributions by installing corner covers produced no difference in the measured Y_W values [3,4]. In addition, high Y_W were measured at the very edge of the antenna box which is geometrically far above the magnetic field lines which connect to antenna straps. This proves that mainly the $E_{||}$-fields at the box require attention to improve AUG antenna.

An $E_{||}$-pattern can be calculated using a number of codes. In our case the HFSS (High Frequency Structure Simulator) code is used. The code provides results for detailed 3D antenna geometry at very high resolution using moderate computer resources. Main limitation of the HFSS is a need to model loads by a medium, which, although can include anisotropy, can not include full plasma dispersion. However, a comparison of HFSS (see Fig. 3a,b) with the TOPICA code [10] (Fig. 3c and [11]) which includes a more realistic plasma model, shows that in both codes high $E_{||}$ are present at AUG antenna limiters, although the exact $E_{||}$-field distribution can depend on properties of the load. $E_y \approx E_{||}$ are shown, because the HFSS anisotropy axis (Fig. 3b) and TOPICA magnetic field (Fig. 3c) are oriented along y. More realistic magnetic

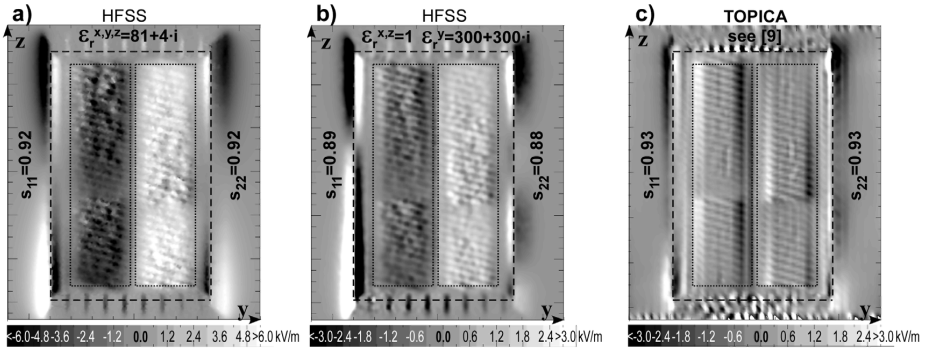

FIGURE 3. Distribution of *Re* (E_y) 2 mm in front of original AUG antenna: *(0π)*-phased straps, curved limiters. Fields normalized to 1 MW coupled using *s*-matrix. Dotted rectangles indicate areas of antenna straps; dashed lines indicate the edges of limiters closest to load. a) HFSS / model with sea water load 60 mm in front of antenna ; b) HFSS / model with plasma-like anisotropic load 20 mm in front of antenna, c) TOPICA / plasma load as described in [9]. Note change of the scale from a) to b).

field angles of 5° to 12 ° to *y*-axis mean a better alignment of magnetic field with the 15° AUG antenna Faraday screen angle. In the cases of the better alignment, calculations yield decreased $E_{||}$-contributions in the areas of the antenna straps (dashed rectangles in Fig.3), particularly where $E_{||}$ due to the RF magnetic flux are located.

Thus, the $E_{||}$-fields which have dipole-like maxima at the limiters which protrude radially and intersect magnetic field lines at large angles of incident are characteristic features in calculations. These $E_{||}$-fields at the limiters contribute strongly to the RF sheath driving voltages [8] responsible for the *W* sputtering which happens on the limiters themselves. This is because the corresponding long magnetic field lines are intercepted by the limiters after they pass the dipole-like field structures only on a single side of a dipole. The $E_{||}$-patterns from Fig.3 are qualitatively inline with the above mentioned experimental observations in AUG [3,4]. A quantitative comparison between the experiments and the calculations is so far incomplete due to a large number of uncertainties both in the experiments (direct measurements of $E_{||}$ are missing) and in the calculations (the dependence of $E_{||}$-distribution on exact load characteristics is present, non-linear effects and the field-plasma self-consistency are missing).

JET A2 four-strap antenna

Another check of consistency of the hypothesis that the $E_{||}$-fields at the box have to be considered as main contributors to the sheath driving voltages for the antennas with radially protruding elements, can be made by using JET data. The JET four strap A2 antennas provide the experimental flexibility with the variation of strap phasings, in particular dipole *(00ππ)*, *(0ππ0)* and *(0π0π)* in the experiments described in [12].

Temperature rise of JET antenna A septum temperature ΔT measured with infra-red camera (Fig. 4a) can be solely attributed to ICRF-related phenomena for the discharges of interest. ΔT, measured as a difference between the temperatures established with and without ICRF heating can be associated with the antenna $E_{||}$-fields [7] and surface RF currents. However ΔT (see Fig. 4b) is also function of septum surface properties and the poloidal distribution of ΔT depends on the distance to the plasma. The latter is presented in Fig.4c as the difference between the septum radial position mapped onto the midplane R_{map} and the midplane position of separatrix R_{sep}. To mini-

mize the influence of these factors, a relative change of the temperature rise $3 \cdot \Delta T_i / \sum_{i=1}^{3} \Delta T_i$, where i is the index of type of dipole phasing. This relative change (Fig. 5a) is compared to the HFSS-produced relative change $3 \cdot V_i / \sum_{i=1}^{3} V_i$

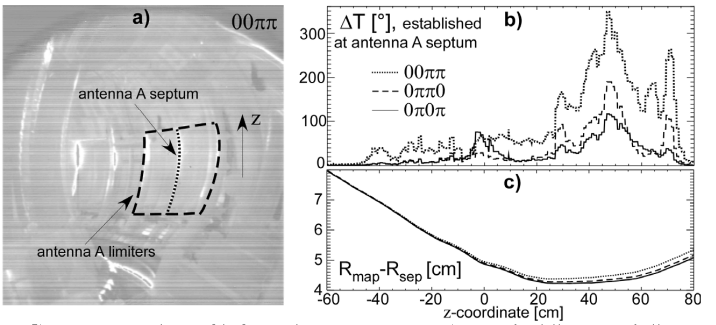

FIGURE 4. a) View of infra-red camera on JET A2 Dashed lines mark limiters, dotted line marks the septum. b) Poloidal profile of temperatures measured for each phasing: 00ππ – #74091, 0ππ0 – #74094 and 0π0π – #74093. c) Antenna-plasma distance corresponding to the discharges.

(Fig. 5b) of RF sheath driving voltage V collected on the field lines which can connect to septum A from the right hand side and averaged over the field lines. Temperature (linearly connected to the septum heat flux) is assumed as linearly connected to the RF voltage [7]. Figure 5 shows that the relative levels of ΔT_i are reasonably reproduced by the levels of V_i. Thus, although the peculiarities of the poloidal distribution are not the same in the experiments and in the modeling (as expected, due to the uncertainties described above), the relative temperature rise on the antenna septum is consistent with the relative change of voltage.

Details of the A2 antenna CAD model used for HFSS calculations are presented in Fig. 6a together with $Re(E_{||})$ contour plots for each type of dipole phasing in Fig.6b,c,d. The $E_{||}$-fields at the limiters and at the septum (marked by the dashed lines) dominate over the fields in front of the antenna straps (dotted areas), especially in the case considered, because the realistic projection of the fields inclined by 11° is taken, i.e. only at 4° misalignment with the FS. Only the ***(0π0π)*** phasing has little fields at the antenna septum, i.e. less ohmic heating by the RF currents on the septum. This might explain a somewhat lower ΔT relative level than the V level for this phasing for low and high z positions as seen in Fig. 5.

The original phasing experiments [12] studied ICRF heating efficiency which relies on the balance between the core and the parasitic edge absorption of ICRF power. On the edge side, apart from the part of $k_{||}$ power spectrum not absorbed centrally, an additional parasitic power is dissipated due to the $E_{||}$-fields. The variavariation of A2 antenna phasing changes both $k_{||}$ and $E_{||}$. Thus the study on the $E_{||}$-pattern supports the efficiency

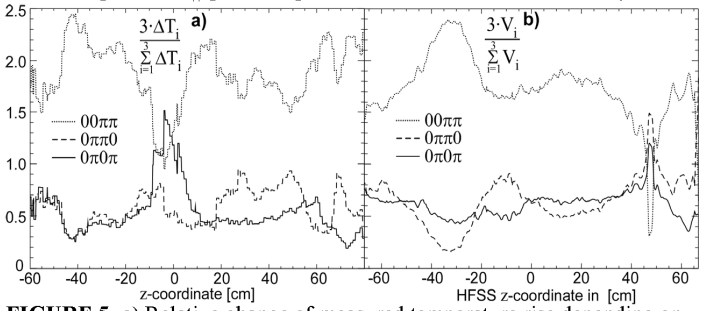

FIGURE 5. a) Relative change of measured temperature rise depending on type of dipole phasing. b) Relative change of HFSS-calculated RF sheath driving voltage collected by the field lines connected to the septum.

study, because the $E_{||}$-fields can affect the balance significantly. The efficiency study [12] shows the consistency that the fraction of the power found in the plasma is lower at a higher level of the V and $E_{||}$-fields from the HFSS calculations (Fig. 5, 6).

The mentioned consistencies encourage further use of the calculations to develop general ways of reduction of the $E_{||}$-fields, and in particular of the $E_{||}$-fields at the box.

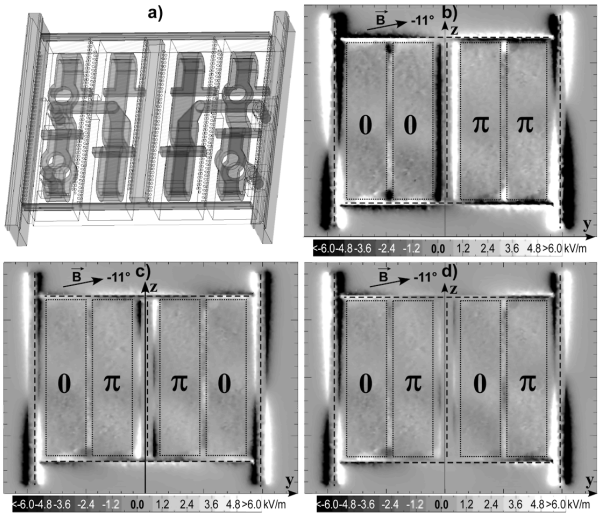

FIGURE 6. a) Model of JET A2 antenna in HFSS with radially protruding limiters and septum. b,c,d) Distribution of *Re* ($E_{||}$) 3 mm in front of the antenna for 1 MW and various phasings.

GUIDELINES TO REDUCE $E_{||}$

The $E_{||}$-fields at the radially protruding elements are due to the existence of image RF currents on the elements, as shown in Fig.7 for original AUG antenna. To reduce the fields, generally one should avoid protruding elements which carry the RF currents, in particular where the currents divert to the direction parallel to the magnetic field. Thus, a septum usually implemented to break up the magnetic field line connections with the aim to decrease the sheath driving voltage [8], can be often counterproductive, like for ***(00ππ)***, ***(0ππ0)*** phasing of JET A2 antenna in Fig.6.

Avoidance of the protruding antenna components in existing experiments is usually not possible. For example in AUG, the antenna limiters are main plasma limiting structures. To reduce $E_{||}$ in this case, changes to the circuit of image currents (Fig.7) should be made in such a way that the surfaces which intersect magnetic field lines carry little or no parallel RF image currents.

One of the approaches is suppressing the parallel currents flowing on the upper and lower parts of the antennas and on the FS by making slots in horizontal septa and in the FS [13].

We address another approach which relies on short circuiting of RF image currents, such that the toroidal (parallel) RF currents close on the poloidal RF currents by providing large-area poloidal connections. The essential condition is that this short circuiting of the currents should occur on the antenna elements which do not intersect magnetic field lines or intersect them at small angles of incidents (few °).

Figure 8b shows a possible realization of the

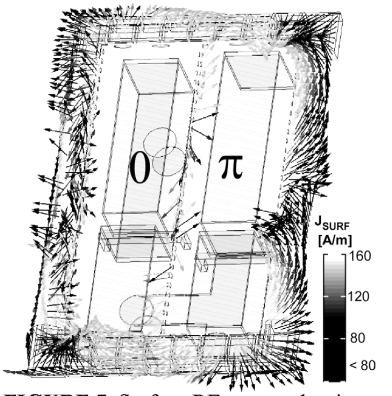

FIGURE 7. Surface RF current density (integrated over the skin-depth) for 1 MW coupled power on the original AUG antenna face excluding FS rods.

approach for AUG and compares its geometry and contour plots of $Re(E_{||})$ to the original AUG antenna in Fig.8a. The modified antenna includes: broader limiters (1) split into two on the left side for compatibility with surrounding in-vessel components; poloidal stripes (2) to allow poloidal RF currents to flow on the slotted limiters (a more solid connection would be preferable, but is not possible); poloidal short circuits (3) (behind the FS) which carry a large fraction of poloidal image currents; bias-cut straps (4) to increase distance between straps and protruding limiters and to decrease image currents on the limiters. The introduction of bias-cut straps makes a compromise on coupling by about 25%. The space inside of the antenna is used for the optimization, because the in-vessel components on the sides of the antennas can not be made non-protruding for AUG due to diagnostic ports etc. It is mainly the components (1), (2) and (3) which provide the short circuiting of the currents and an improvement in terms of sheath driving voltage. According to the HFSS calculations, RF sheath driving voltages on the long field lines passing in front of the antennas are reduced by about a factor of 2. To a large extent this reduction is due to the overall reduction of $E_{||}$. Average $E_{||}$-level (integrated over the whole plane) is reduced by a factor of 1.34.

Among other options left out of the modified antenna in Fig. 8, can be installation of continuous structures elongated along magnetic fields lines (e.g. toroidal limiters) just at the sides of the antenna limiters. This enforces $E_{||}$=0 boundary condition and reduces the fields.

In the case of four-strap antennas (and generally an antenna with more than 2 straps), a better balance between *(0π)*–phase contributions can be found [4]. This means that RF image currents of one strap can be compensated by the image currents out-of-phase. However, as Fig.3 suggests, the balance can be load-dependent so that RF currents in all poloidal locations might not be balanced for all conditions.

In the case the protruding antenna limiters can be avoided and antenna can be integrated in a wall (i.e. no box fields), the RF sheath driving voltages on the shorter field

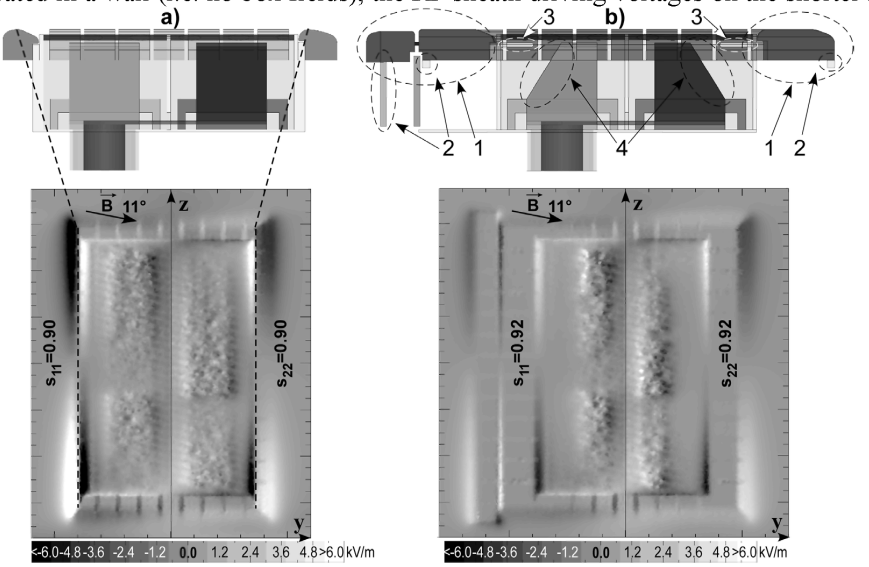

FIGURE 8. Side view of antennas with corresponding 1 MW-$Re(E_{||})$ contour plots from HFSS for a sea water load 4 cm in front of antenna. a) Original AUG antenna. b) Proposed modified antenna.

lines which are enclosed between FS rods, become important [8]. In this case the best alignment of magnetic field with FS should be achieved. Applied to the optimization of ITER antenna design [14], a single "flat" FS with the inclination angle of 15° would have the advantage of lower $E_{||}$ over the antenna with horizontal individual FSs where the FSs are protruding radially. The protruding FSs lead to increased $E_{||}$-fields on their boundaries, similar to how the box does [15].

CONCLUSIONS

It has been shown, that the conditions required to reduce the ICRF-related impurity problem which is strongly dependent on light impurity content in the plasma, are not necessarily those required to reduce the ICRF-related heat flux problem, although both problems are to a large extent due to $E_{||}$-fields. For AUG and JET A2 antennas, the $E_{||}$-fields originate from image currents on radially protruding antenna PFCs such as limiters and septa which intersect magnetic field lines at large angles of incident. To reduce $E_{||}$, the protruding structures with RF image currents should be avoided where possible. For AUG antenna, where the antenna limiters can not be avoided, short-circuiting of the image currents is proposed by using broadened limiters and solid poloidal connections to close the toroidal (parallel) currents via poloidal currents. Other options like continuous structures elongated along magnetic field and a good balance between *(0π)*-phased contributions to the image currents for antenna with more than 2 straps help reducing the $E_{||}$-fields. To minimize $E_{||}$-fields at the ITER-antenna, protruding individual Faraday screens can be replaced by a single flat FS while the rods of the FS could be 15° inclined to avoid $E_{||}$ at the antenna straps.

ACKNOWLEDGMENTS

The authors would like to thank Dr. Ph. Lamalle for providing an adapted CAD model of JET A2 antenna.

This work, supported by the European Communities under the contract of Association between EURATOM and IPP, was carried out within the framework of EFDA. The views and opinions expressed herein do not necessarily reflect those of the European Commission.

REFERENCES

1. R. Neu, *Plasma Phys. Control. Fusion* **49, 12B** B59 (2007).
2. A. Kaye et al., *Fusion Eng. Des.*, **74**, 1-21 (1994).
3. V. Bobkov et al., *J. Nucl. Mater* **390-391**, 900-903 (2009).
4. V. Bobkov et al., *submitted to Nuclear Fusion.*
5. R. Dux et al., *J. Nucl. Mater* **390-391**, 858-863 (2009).
6. V. Bobkov et al., *J. Nucl. Mater* **363-365**, 122-126 (2007).
7. L. Colas et al., *this conference.*
8. J. R. Myra et al., *Fusion Eng. Des.* **31** 291 (1996).
9. L.Colas et al, *Nucl. Fusion* **45** 767 (2005).
10. V. Lancelotti et al., *Nucl. Fusion* **46** S476 (2006).
11. A. Krivska et al., *this conference.*
12. E. Lerche et al., *this conference.*
13. A.. Mendes et al., *this conference*
14. D. Milanesio and R. Maggiora, *to be submitted to Nuclear Fusion.*
15. L.Colas et al., *J. Nucl. Mater* **390-391**, 959-962 (2009).